Applying a Bayesian Approach to Identification of Orthotropic Elastic Constants from Full Field Displacement Measurements

C. Gogu[1,2,a], W. Yin[2], R. Haftka[2], P. Ifju[2], J. Molimard[1], R. Le Riche[1], and A. Vautrin[1]

[1]Ecole des Mines de Saint Etienne, Centre Sciences des Matériaux et des Structures, 158 cours Fauriel, 42023 Saint Etienne cedex 2, France
[2]University of Florida, Mechanical and Aerospace Engineering Department, PO Box 116250, Gainesville, FL 32611, USA

Abstract. Full field displacement measurements offer the potential of identifying several elastic properties together. However, the complexity of the approach means that quantifying the uncertainty in the identified properties is less straight forward. Here, Bayesian identification is attractive, because it can readily model all the uncertainties in the analysis and measurements, and in addition it provides the full coupled probability distribution of the identified elastic constants. This is demonstrated here by using full-field displacement measurements of an orthotropic plate with an open hole to identify the elastic constants. One of the barriers to the application of Bayesian identification is the computational burden associated with very large vectors of measurements. This is addressed by the use of proper orthogonal decomposition for reducing the dimensionality of the measurements and expensive finite element simulations. The identified probability distribution of the four orthotropic elastic constants showed that these are determined with quite different confidence levels as well as with significant correlation. Comparison with manufacturing specifications showed substantial difference in one constant, and this conclusion agreed with earlier measurement of that constant by a traditional four-point bending test.

1 Introduction

For identifying orthotropic elastic constants, methods based on full field strain or displacement measurements are gaining popularity [1], since they allow to capture the fields' non-uniformity. This information offers the potential of identifying all four elastic constants from a single experiment. It requires though a more complex identification framework compared to traditional point-wise tests on unidirectional specimen.

Numerous improvements in identification methods have provided increasingly accurate estimates of the material properties involved. However, characterizing the uncertainty in the identified properties is still relatively crude, especially for complex experiments. This is important however, since different material properties obtained from a single test are not identified with the same

---

confidence. Typically the highest uncertainty is associated with respect to properties to which the experiment is the most insensitive. In addition, the uncertainty in different properties can be strongly correlated, so that obtaining only variance estimates may be misleading.

Thus one of the current challenges in the identification of multiple material properties from a complex experiment resides in handling different sources of uncertainty in the experiment and the modelling of the experiment for estimating the resulting uncertainty in the identified properties.

A possible approach for doing this is the Bayesian method [2],[3]. This method was introduced in the late 1970s in the context of identification [4] and has been applied since to different problems, notably identification of elastic constants from plate vibration experiments [5]-[7]. The applications of the method to these classical point-wise tests involved only a small number of measurements (typically ten natural frequencies in the previously cited vibration test), which facilitated the application of the Bayesian approach.

In the present article we identify the orthotropic elastic constants of a composite material from an open hole tensile test on a laminate, on which we measure the *U* and *V* displacement fields. Several authors carried out identifications based on such measurements within a least squares framework [8],[9]. We propose here to apply the Bayesian identification approach. This is of particular interest with full field measurements, since they provide a large amount of data (one displacement measurement per pixel of the image) and hence a promise of smaller uncertainties in the identified properties. However, the high number of measurements represents also a major computational challenge in applying the Bayesian approach to full field measurements.

To address this challenge we propose an approach based on the proper orthogonal decomposition (POD) of the full fields in combination with response surface methodology (RSM). POD is used in order to drastically reduce the dimensionality of the data to computationally more manageable levels, while RSM is used to reduce the computational cost of the statistical sampling needed for the Bayesian implementation.

The rest of the paper is organized as follows. In Section 2 we give an overview of the identification problem from an open-hole tensile test as well as the Moiré interferometry experiment that was carried out. In Section 3 we apply proper orthogonal decomposition (POD) to the full fields, while in Section 4 we construct response surface approximations of the POD coefficients. Section 5 provides the Bayesian identification formulation and results. We give concluding remarks in Section 6.

2 Open hole tensile test

2.1 Experiment

In this paper we consider the identification of orthotropic ply-elastic constants from full field displacement measurements on an open hole plate. The plate is a laminate fabricated from a graphite/epoxy prepreg (Toray[®] T800/3631) with a stacking sequence of [45,-45,0]$_s$. Prior information on the properties that we seek was available from the manufacturer and from previous experiments. The manufacturer's specifications are given in Table 1 together with the properties obtained by Noh [18]. Noh obtained the material properties based on a four points bending test at the University of Florida on a laminate made from the exact same prepreg roll that we used in the full field open hole test.

Table 1. Manufacturer's specifications and properties found by Noh [18] based on a four points bending test.

Parameter	E_1(GPa)	E_2 (GPa)	ν_{12}	G_{12} (GPa)
Manufacturer's specifications	162	7.58	0.34	4.41
Noh's values [18]	144	7.99	0.34	7.78

In the present study we seek to identify the ply-properties and their uncertainties from a tensile test on a laminate having the dimensions given in Figure 1. The total thickness h is 0.78 mm and the applied tensile force 700 N. The U and V displacement fields are defined as being in the 1, respectively 2 direction. The full field measurements are taken on a square area 24.3 x 24.3 mm^2 around center of the hole. The tensile force applied is 700 N.
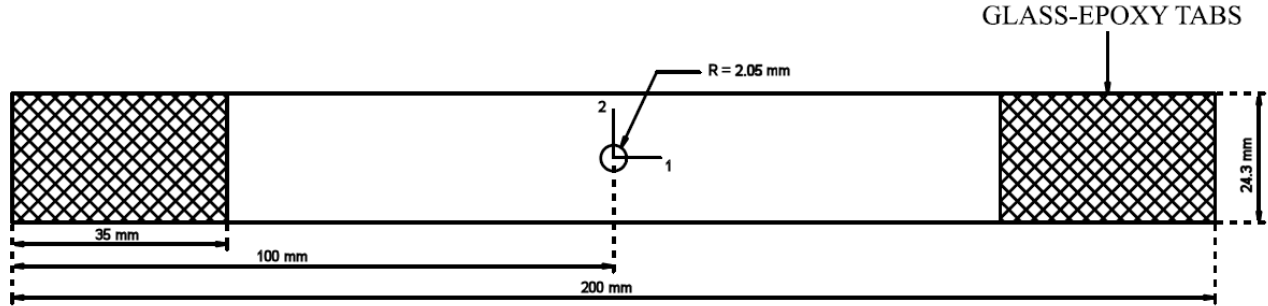

Figure 1. Specimen geometry. The specimen material is graphite/epoxy and the stacking sequence [45,-45,0]$_s$. The tensile force is 700 N.

Moiré interferometry was used in this study to measure the displacement fields. Moiré interferometry is a technique utilizing the fringe patterns obtained by optical interference off a diffraction grating in order to obtain full field displacement maps. For a detailed description of the method and some of its applications refer to [10]. Among the main advantages of Moiré interferometry are its high signal to noise ratio, its excellent spatial resolution and its insensitivity to rigid body rotations [11]. The displacement resolution, obtained by repeatability tests, can be as low as 4 nm.

For the measurements we used a diffraction grating with 1200 lines/mm, that was transferred onto the specimen. An ESM Technologies PEMI II 2020-X Moiré interferometer using a Pulnix TM-1040 digital camera were utilized. The traction machine was an MTI-30K. Rotations of the grips holding the specimen were allowed by using a lubricated ball bearing for the bottom grip and two lubricated shafts for the top grip. This allowed to reduce parasitic bending during the tension test. The experimental setup is shown in Figure 2.
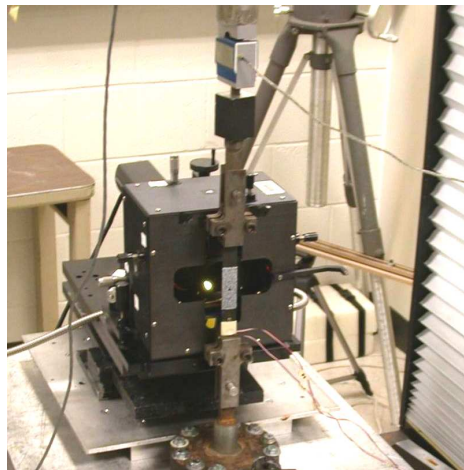

Figure 2. Experimental setup for the open hole tension test.

The phase shifting method was used to extract the displacement fields from the fringe patterns. A Matlab automated phase extraction tool developed by Yin [12] was utilized and the displacement maps extracted from the fringe patterns are provided in Figure 3. Note that no filtering whatsoever was used during the extraction algorithm. These two displacement fields serve as the measurements for the present identification problem.

Typical sources of uncertainty affecting the displacement fields are noise, the phase extraction procedure, imperfect centering of the hole on the specimen or misalignment of the grips, which can create bending.
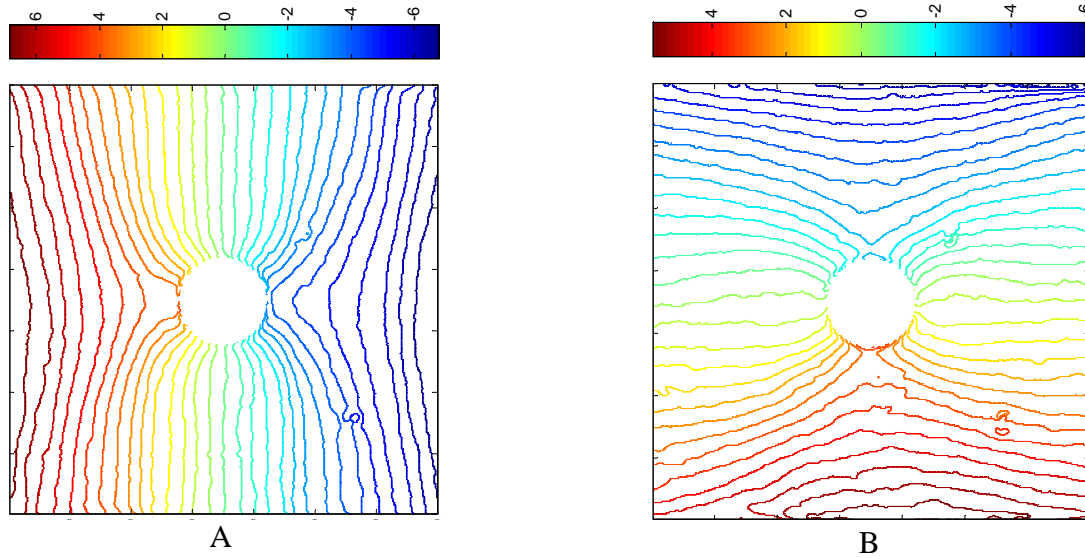

Figure 3. Displacement fields (in µm) obtained from the fringe patterns in: A) The *U* direction. B) The *V* direction.

2.2 Modelling and problem statement

In order to identify the ply-elastic constants, E_1, E_2, v_{12}, G_{12}, we need a model relating these to the displacement fields. Unfortunately there are no exact analytical solutions for the problem of an orthotropic plate. Instead we chose a finite element model for this purpose.

The plate is modeled using the Abaqus® finite element software. A total of 8020 S4R elements (general purpose, four nodes per element, reduced integration) were used. The finite element mesh in the area of interest is shown in Figure 4 and the measurement area highlighted in red. Note that Figure 4 does not include the entire mesh. Since the whole plate is modeled in Abaqus there is a transition using triangular elements towards a larger mesh at the grip edges of the plate where the stresses are relatively uniform compared to the area around the hole.

A finite element mesh convergence study was carried out, and it was found that with the present mesh the discretization error in the area of interest was of the order of 6×10^{-4} % of the average absolute value of the field, which was considered acceptable.
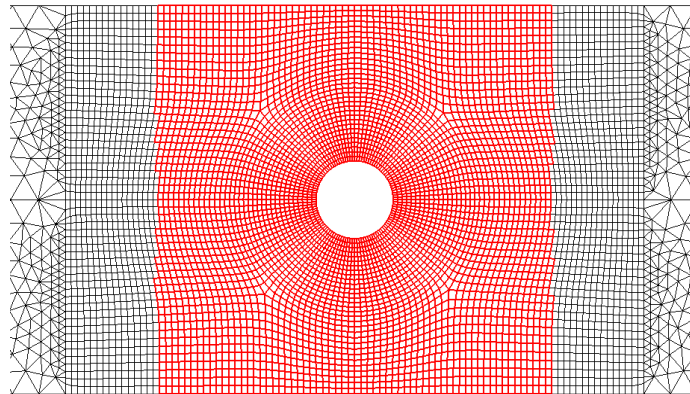

Figure 4. Finite element mesh. The measurement area is highlighted in red.

During the identification process we vary a certain number of model parameters such as elastic constants or plate dimensions and obtain each time the corresponding full fields. We seek to match the predictions with the experimental fields either in a deterministic way (least squares) or in a probabilistic way (Bayesian) as we will propose here.

The field is described here by the displacement values at the 4569 nodes within the reference area (see highlighted area in Figure 4). Note that the experimental fields contain much more information, since we obtain 490,000 measurement points (pixels) per field. The values of the experimental fields at the node positions are thus calculated by linear interpolation.

If a field calculation needs to be used within the Bayesian framework where correlation between the measurements is required, it is not practical to describe the fields by their value at each point (at the 4569 nodes here). This is essentially because thousands-dimensional probability density functions required to describe the correlation between the different measurement points are outside the realm of what the statistical methods can currently handle with reasonable computational resources.

Furthermore the model evaluation needs to be repeated millions of times during the identification, problem exacerbated by the need for statistical sampling. Using a finite element model directly is not computationally feasible in this case.

The computational challenge can then be stated as follows. First, can we find a reduced dimensional representation of the full fields for whatever combination of input parameters (elastic constants, plate dimensions in our case) within a certain domain? Second, can we reduce the cost required for the model evaluation?

To address these problems we propose to use the proper orthogonal decomposition method for dimensionality reduction and response surface methodology for cost reduction. These are described in the following two sections.

3 Proper orthogonal decomposition

3.1 Theoretical foundations

Let us consider $U^i \in \mathbb{R}^n$, which is the vector representation of a field (e.g. displacement field). Note that n is usually several thousands. We seek, based on N sample vectors $\{U^i\}_{i=1..N}$, a reduced dimensional representation of the fields' variations with some input parameters.

The aim of the proper orthogonal decomposition (POD) method is to construct an optimal, reduced dimensional basis for the representation of the sample vectors (also called snapshots). In the POD approach the snapshots need to have zero mean, if this is not the case the mean value needs to be subtracted.

We denote $\left\{\boldsymbol{\Phi}_k\right\}_{k=1..K}$ the vectors of the orthogonal basis of the reduced dimensional representation of the snapshots. The POD method seeks to find the basis vectors $\boldsymbol{\Phi}_k$ that minimize the representation error:

$$\min \frac{1}{2} \sum_{i=1}^{N} \left\| U^i - \sum_{k=1}^{K} \alpha_{i,k} \boldsymbol{\Phi}_k \right\|_{L2}^2 \tag{1}$$

Because $\left\{\boldsymbol{\Phi}_k\right\}_{k=1..K}$ is an orthogonal basis, the coefficients $\alpha_{i,k}$ are given by the orthogonal projection of the snapshots onto the basis vectors. As a result we have the following reduced dimensional representation $\widetilde{U}^i$ of the vectors of the snapshot set:

$$\widetilde{U}^i = \sum_{k=1}^{K} \alpha_{i,k} \boldsymbol{\Phi}_k = \sum_{k=1}^{K} \left\langle U^i, \boldsymbol{\Phi}_k \right\rangle \boldsymbol{\Phi}_k \tag{2}$$

The reduction in dimension is from N to K. The truncation order K needs to be selected such as to maintain a reasonably small error in the representations $\widetilde{U}^i$ of U^i. Selecting such a K is always problem specific and an error criterion is given further down.

The main advantage of the POD method is that it provides a simple procedure for constructing the basis from the samples $\{U^i\}_{i=1..N}$. The procedure guarantees that for a given truncation order we cannot find any other basis that better approximates the snapshots subspace.

The basis $\left\{ \mathbf{\Phi}_k \right\}_{k=1..K}$ is constructed using the following matrix:

$$X = \begin{pmatrix} U_1^1 & \cdots & U_1^N \\ \vdots & \ddots & \vdots \\ U_n^1 & \cdots & U_n^N \end{pmatrix} \tag{3}$$

The vectors $\left\{ \mathbf{\Phi}_k \right\}_{k=1..K}$ are then obtained by the singular values decomposition of X, or equivalently by calculating the eigenvectors of the matrix XX^T. The singular values decomposition allows writing that:

$$X = \Phi\Sigma\Lambda^T \tag{4}$$

where Φ is the matrix of the column vectors $\mathbf{\Phi}_k$. The *svd()* function in Matlab was used here for the singular value decomposition.

A truncation error criterion ε is then defined by the sum of the error norms as shown in Equation 5.

$$\sum_{i=1}^{N} \left\| U^i - \sum_{k=1}^{K} \alpha_{i,k}\mathbf{\Phi}_k \right\|_{L2}^2 \leq \varepsilon \sum_{i=1}^{N} \left\| U^i \right\|_{L2}^2 \tag{5}$$

where $\varepsilon = 1 - \left(\sum_{j=1}^{K} \sigma_j^2 \bigg/ \sum_{j=1}^{N} \sigma_j^2 \right)$, and σ_j are the diagonal terms of the diagonal matrix Σ. For a derivation of this criterion and further details on POD the reader can refer to [13].

3.2 POD decomposition of the full fields

For the open hole plate identification problem we are interested in accounting for variations of the following parameters: ply elastic constants E_1, E_2, v_{12}, G_{12} and ply thickness t. We are looking at variations of the homogenized ply-properties and thickness here and not at spatial variations within the plate. Accounting for variations in the elastic constants is needed as usual for the identification procedure. We added here the ply thickness to illustrate a typical source of uncertainty that the Bayesian identification can account for. We assumed here that we are interested in variations of the parameters E_1, E_2, v_{12}, G_{12} and t within the bounds given in Table 2.

Table 2. Bounds on the input parameters of interest (for a graphite/epoxy composite material).

Parameter	E_1 (GPa)	E_2 (GPa)	v_{12}	G_{12} (GPa)	t (mm)
Lower bound	126	7	0.189	3.5	0.12
Upper bound	234	13	0.351	6.5	0.18

We obtained the snapshots required for the POD approach by sampling 200 points within the bounds of Table 2. The points are obtained by Latin hypercube sampling, which consists in obtaining the 200 sample points by dividing the range of each parameter into 200 sections of equal marginal probability 1/200 and sampling once from each section. Latin hypercube sampling typically ensures that the points are reasonably well distributed in the entire space.

At each of the 200 sampled points we perform a finite element analysis, which gives the corresponding horizontal and vertical displacement fields U and V respectively. Each of the 200 fields of U (and 200 of V) represents a snapshot and is stored as a column vector that will be used for the POD decomposition. The simulated measurement area (see highlighted area in Figure 4) covers 4569 finite element nodes so we obtain snapshots vectors of size 4569 x 1. The snapshots matrix X has then a size of 4569 x 200. Note that as mentioned in the POD theory section, the snapshots need to have zero mean. In our case this was true for the U field but not for the V field, so we needed to subtract the mean value of each snapshot as shown in Equation 6, where the bar notation denotes the mean value of the field.

$$X = \begin{pmatrix} V_1^1 - \overline{V}_1 & \cdots & V_1^N - \overline{V}_N \\ \vdots & \ddots & \vdots \\ V_n^1 - \overline{V}_1 & \cdots & V_n^N - \overline{V}_N \end{pmatrix} \tag{6}$$

The POD modes of the 200 fields are then calculated using the singular value decomposition as shown in Equation 4. Note that there are two potential ways to do the POD decomposition: on U and V independently or on U and V together (i.e. a single vector of size 9138 x 1). With U and V together we have for a given truncation order half as many degrees of freedom as with U and V independently. While for a given truncation order the error using U and V together is smaller, we found that it is more difficult in this case to construct response surface approximations (RSA) of the POD coefficients due to higher errors in the RSA. Since for the identification we will need to construct RSA we chose to do the POD decomposition on U and V independently.

An illustration of the fields obtained for a particular snapshot (snapshot 1) is shown in Figure 5, which provides an idea of the spatial variations and order of magnitude of the fields. These fields were obtained with the following parameters: E_1=202.2 GPa, E_2=10.84 GPa, v_{12}=0.2142, G_{12}=4.989 GPa, t=0.1312 mm.
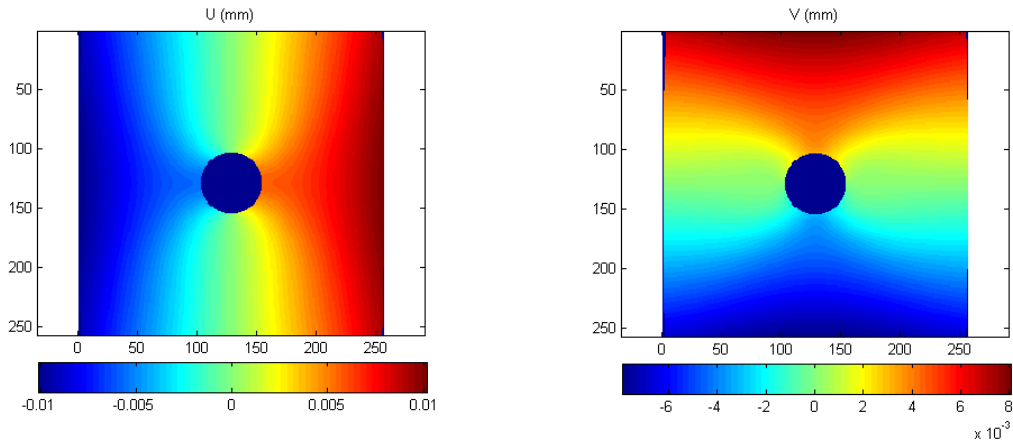

Figure 5: *U* and *V* displacement fields for snapshot 1.

In total we obtained 200 POD modes. The first four are represented graphically in Figures 6 and 7. We note that the first modes are relatively close (but not identical even though the differences cannot be seen by naked eye) to the typical U and V displacement fields (see Figure 5). Furthermore we see that the modes have a more complicated shape with increasing mode number, as expected for a modal decomposition basis. For additional details on the POD decomposition of the open hole tensile test full fields the reader can refer to [14].
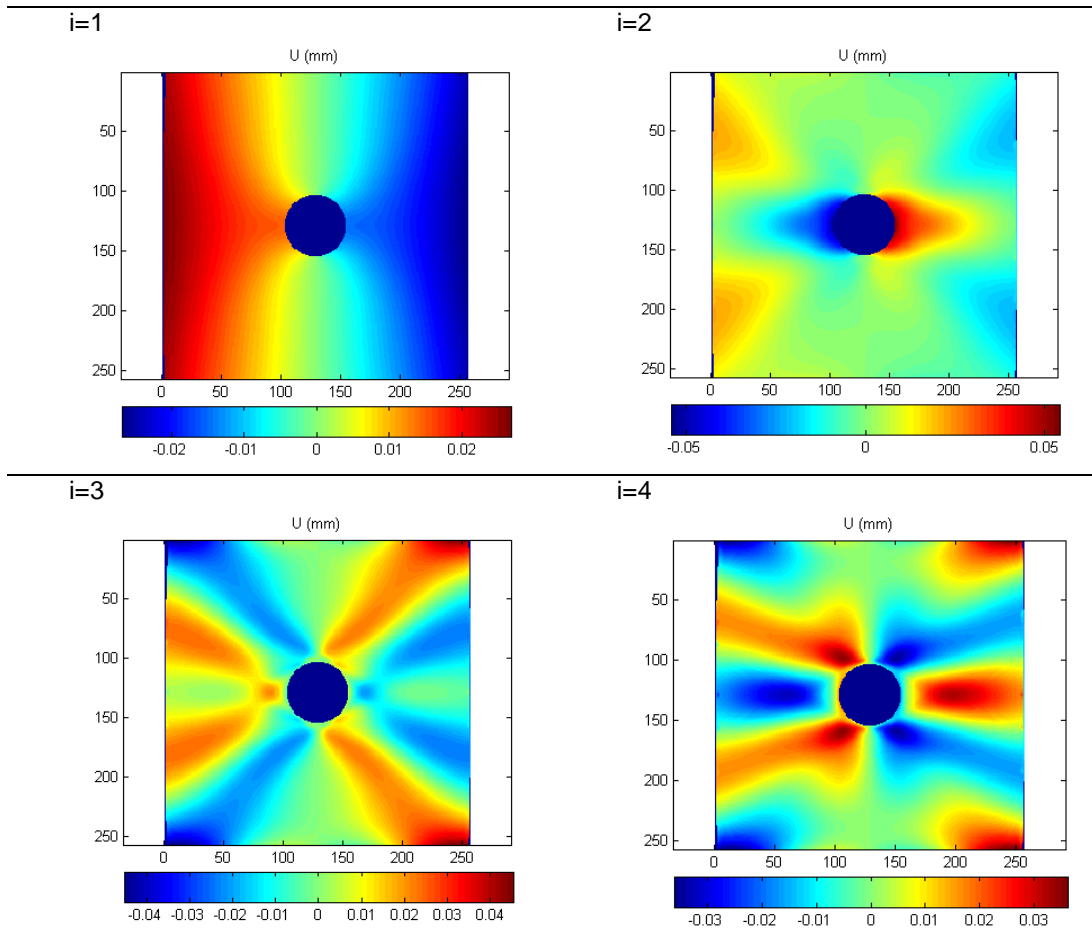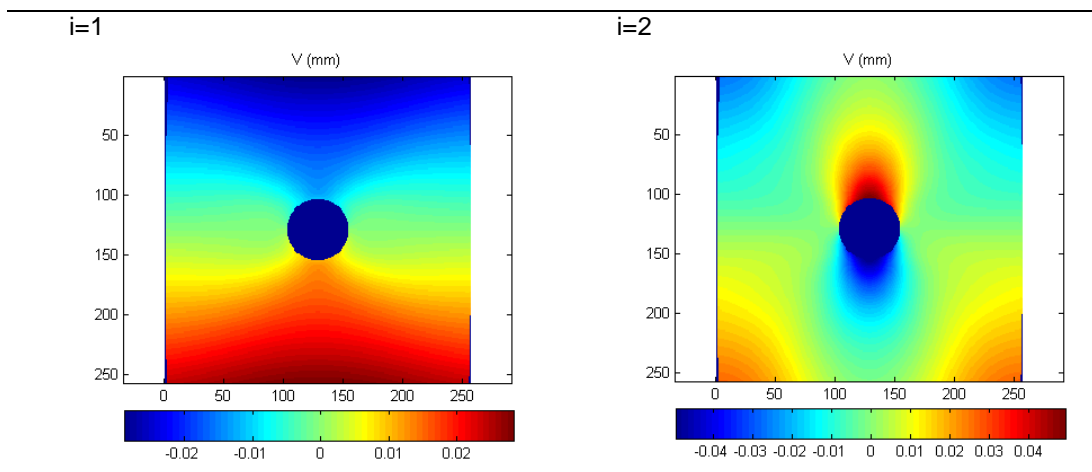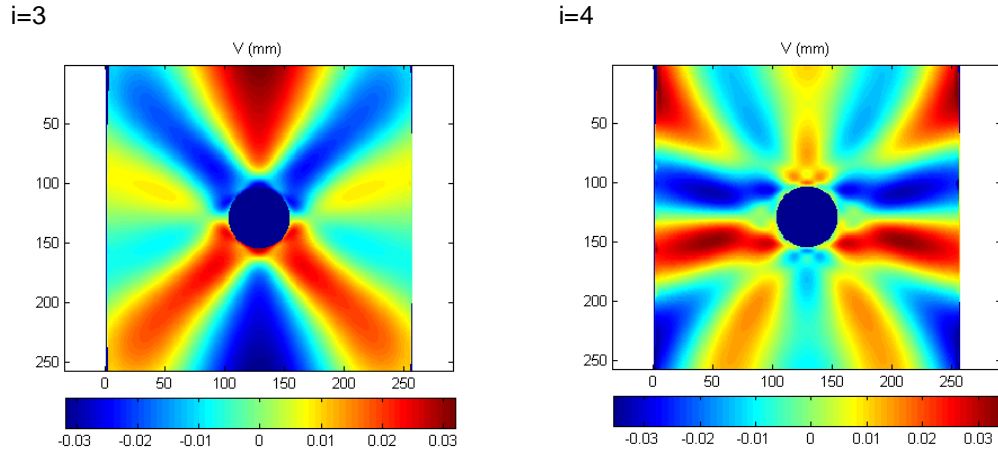
i=1

i=2

i=3

i=4

Figure 6: First 4 POD modes for the *U* field.

i=1

i=2

i=3   i=4

Figure 7: First 4 POD modes for the *V* field.

Once the POD modes determined we need to find an appropriate truncation order *K* for the reduced dimensional approximations of the fields (see Equation 2). Table 3 provides the truncation error criterion defined in Equation 5.

Table 3. Error norm truncation criterion (ε is defined in Equation 5).

K	2	3	4	5
ε for U fields	2.439×10^{-7}	4.701×10^{-9}	7.280×10^{-11}	1.211×10^{-11}
ε for V fields	1.054×10^{-6}	2.900×10^{-9}	4.136×10^{-10}	3.517×10^{-11}

The error norm truncation criterion ε, while being a global error criterion, is relatively hard to interpret physically. Furthermore the criterion is based only on the convergence of the snapshots that served for the POD basis construction. However in most cases we will want to decompose a field that is not among the snapshots, so we also want to know the convergence of the truncation error in such cases.

Accordingly we chose to construct a different error measure based on cross validation. The basic idea of cross validation is the following: if we have *N* snapshots, instead of using them all for the POD basis construction we can use only *N*-1 snapshots and compute the error between the actual fields of the snapshot that was left out and its truncated POD decomposition. By successively changing the snapshot that is left out we can thus obtain *N* errors. The root mean square of these *N* errors, which we denote by CV_{RMS}, is then a global error criterion that can be used to assess the truncation inaccuracy.

In order to use the cross validation technique we need to define how to measure the error between two strain fields (the actual strain field and its truncated POD decomposition). We chose the maximum absolute difference between two fields. This maximum error is computed at each of the *N* (*N*=200 here) cross validation steps and the root mean square leads to the global error criterion CV_{RMS}. Table 4 provides these values for different truncation orders. The relative CV_{RMS} error with respect to the value of the field where the maximum error occurs is also given in Table 4.

Table 4. Cross validation CV_{RMS} truncation error criterion.

	K	2	3	4	5
U field	CV_{RMS} (mm)	9.35×10^{-6}	1.05×10^{-6}	1.65×10^{-7}	7.83×10^{-8}
	CV_{RMS} (%)	9.96×10^{-2}	1.13×10^{-2}	2.37×10^{-3}	9.49×10^{-4}
V field	CV_{RMS} (mm)	1.00×10^{-5}	6.30×10^{-7}	3.05×10^{-7}	7.32×10^{-8}
	CV_{RMS} (%)	1.10×10^{-1}	4.71×10^{-2}	3.71×10^{-3}	1.84×10^{-3}

At this point we make the following remark. Truncating at $K=4$ means that the POD decomposition achieved a dimensionality reduction from 4569 to 4. Such a high reduction might seem surprising but this is because changes in the dimensions and elastic constants exhibit field variations characterized by relatively low dimensionality. When varying the input parameters the variations of a point of the field are obviously not completely independent from the variations of its neighbors. We have found that characterizing these variations in a modal basis of dimensions four already leads to a small error.

Since the fields will be used for identification not only the accuracy of the fields is important but also the accuracy of the derivates of the field with respect to the ply-elastic constants. This was verified and we found that four POD coefficients for each field are also sufficient for representing the derivates accurately enough. For details the reader can refer to [15].

On a final note the identification procedure will use the POD projection of the displacement fields, which will filter out some information present in the initial fields. This can have both positive and negative effects. Obvious negative effects are that the identification procedure will not be able to account for any information that was filtered out and that might have been useful to the identification or the propagation of uncertainties. On the other hand if the information filtered out is mainly related to the analysis tools used (e.g. phase extraction algorithm) it can be useful to leave out these artifacts since they do not have physical meaning in relation to the material properties. An investigation of the errors left out was carried out in [15] (Chapter 7), and we found it is reasonable to do the identification on the POD coefficients.

4 Response surface approximations

Even though we reduced the dimensionality of the full field using the POD decomposition, the calculation of the POD coefficients is up to now still based on finite element results. Since about 700 million evaluations need to be used for the Bayesian identification procedure, finite element simulations remain prohibitive so we will seek to construct computationally cheap approximations of the POD coefficients, α_k, as functions of the four elastic constants to be identified and the thickness of the plate, which has some uncertainty that we want to account for.

For this purpose we use response surface methodology. Response surface methodology or surrogate modeling is a technique used to approximate the response of a structure, which is known only in a finite and usually small number of points. The points where the response is known, which constitute the design of experiments (DoE), are fitted with a particular function depending on the response surface approximation (RSA) type used. A common RSA is the polynomial response surface (PRS), which fits the simulation occurrences from the DoE with a polynomial so as to minimize the square difference between the simulations and the prediction of the PRS. The accuracy of the approximation can then be estimated using indicators such as RMS error or cross validation error. For more details on RSA techniques the reader can refer to [16].

For the present problem we employed response surface approximations for each POD coefficient, of the form $\alpha_k=\text{PRS}(E_1, E_2, v_{12}, G_{12}, h)$. Third degree polynomial response surface approximations were constructed from the same 200 samples that were used in the previous section to construct the POD basis. These 200 points were sampled using Latin hypercube within the bounds given in Table 2.

The error measures used to assess the quality of the RSA fits are given in Table 5 for the first four POD coefficients of the *U* fields and in Table 6 for those of the *V* fields. The second row gives the mean value of the POD coefficient across the design of experiments (DoE). The third row provides the standard deviation of the coefficients across the DoE, which gives an idea of magnitude of variation in the coefficients. Row four provides R^2, the correlation coefficient obtained for the fit, while row five gives the root mean square error among the DoE points. The final column gives the cross validation PRESS error [17].

Table 5. Error measures for RSA of the U-field POD.

POD coefficient RSA	α_1	α_2	α_3	α_4
Mean value of α_i	$-4.04\ 10^{-1}$	$-3.40\ 10^{-5}$	$-2.20\ 10^{-5}$	$-8.35\ 10^{-7}$
Standard deviation of α_i	$8.19\ 10^{-2}$	$6.92\ 10^{-4}$	$2.01\ 10^{-4}$	$2.80\ 10^{-5}$
R^2	0.99999	0.99993	0.99992	0.99951
RMS error	$2.77\ 10^{-4}$	$6.32\ 10^{-6}$	$2.01\ 10^{-6}$	$6.75\ 10^{-7}$
PRESS error	$3.61\ 10^{-4}$	$7.92\ 10^{-6}$	$2.67\ 10^{-6}$	$9.33\ 10^{-7}$

Table 6. Error measures for RSA of the V-field POD.

POD coefficient RSA	α_1	α_2	α_3	α_4
Mean value of α_i	$-2.97\ 10^{-1}$	$-9.51\ 10^{-5}$	$-2.14\ 10^{-5}$	$9.76\ 10^{-7}$
Standard deviation of α_i	$5.40\ 10^{-2}$	$2.26\ 10^{-3}$	$3.10\ 10^{-4}$	$1.50\ 10^{-5}$
R^2	0.99999	0.99992	0.99987	0.99830
RMS error	$1.69\ 10^{-4}$	$2.26\ 10^{-5}$	$3.88\ 10^{-6}$	$6.89\ 10^{-7}$
PRESS error	$2.45\ 10^{-4}$	$3.05\ 10^{-6}$	$5.27\ 10^{-6}$	$1.04\ 10^{-6}$

Comparing the error measures to the standard deviations of the coefficients we considered that the RSA are accurate enough to be used in the identification process, with the approximation error being negligible compared to the other sources of uncertainty.

5 Bayesian identification

5.1 Bayesian formulation

In Bayesian identification we seek to identify the joint probability distribution of the elastic constants E_1, E_2, v_{12}, G_{12} given the measured displacement fields on the open hole plate. Denoting by f probability density functions (PDF), then the PDF that we seek, also called posterior PDF, is given by Bayes' formula:

$$f_{E/\alpha=\alpha^{measure}}\left(\boldsymbol{E}\right) = \frac{1}{K} f_{\alpha/E}\left(\boldsymbol{\alpha}^{measure}\right) \cdot f_E^{prior}\left(\boldsymbol{E}\right) \tag{7}$$

where $\boldsymbol{E} = \{\ E_1,\ E_2,\ v_{12},\ G_{12}\}$ is the four dimensional random variable of the ply-elastic constants. $\boldsymbol{\alpha} = \left\{\alpha_1^U,...,\alpha_4^U,\alpha_1^V...\alpha_4^V\right\}$ is the eight dimensional random variable of the POD coefficients of the $\boldsymbol{U}$ and $\boldsymbol{V}$ field. $\boldsymbol{\alpha}^{measure} = \left\{\alpha_1^{U,measure},...,\alpha_4^{U,measure},\alpha_1^{V,measure}...\alpha_4^{V,measure}\right\}$ is the vector of the eight "measured" POD coefficients, obtained by projecting the measured full fields onto the POD basis.

Equation 7 provides the joint probability density function (PDF) of the four elastic constants given the coefficients $\boldsymbol{\alpha}^{measure}$. This PDF, also called posterior PDF and denoted $f_{E/\alpha=\alpha^{measure}}\left(\boldsymbol{E}\right)$, is equal to a normalizing constant times the likelihood function of the elastic constants $\boldsymbol{E}$ given the coefficients $\boldsymbol{\alpha}^{measure}$ times the prior distribution of the elastic constants $\boldsymbol{E}$.

The prior distribution of $\boldsymbol{E}$ reflects the prior knowledge we have on the elastic constants based on manufacturer's specifications for example. The mean value of the distribution was based on the manufacturer's specifications for the Toray® prepreg. We assumed that we have relatively vague prior knowledge by defining a joint uncorrelated normal prior distribution with relatively wide standard deviations (10%) as defined in Table 7. The prior distribution was truncated at the bounds given in Table 8, which were chosen in an iterative way such that eventually the mean of the

posterior PDF is approximately in the center of the bounds and their range covers approximately four standard deviations of the posterior PDF.

Table 7. Normal uncorrelated prior distribution of the material properties for a graphite/epoxy composite material.

Parameter	E_1(GPa)	E_2 (GPa)	ν_{12}	G_{12} (GPa)
Mean value	162	7.58	0.34	4.41
Standard deviation	16	0.75	0.03	0.5

Table 8. Truncation bounds on the prior distribution of the material properties

Parameter	E_1(GPa)	E_2 (GPa)	ν_{12}	G_{12} (GPa)
Lower truncation bound	126	6	0.26	4.25
Upper truncation bound	151	9.5	0.36	5.75

The other term on the right hand side of Equation 7 is the likelihood function of the elastic constants given the POD coefficients $\boldsymbol{\alpha}^{measure}$. This function provides an estimate of the likelihood of different $\boldsymbol{E}$ values given the test results.

The uncertainty in the POD coefficients can have several causes, which are detailed next. A typical cause of uncertainty in the problem is measurement error. In the case of full field measurements we usually obtain a noisy field, which can possibly be decomposed into a signal component and a white noise component. We showed in [15] that a Gaussian white noise on the full fields can be modeled by Gaussian distributions on the POD coefficients, having zero mean and the same standard deviation as the noise on the fields. Note that this does not mean that there is no filtering effect through the use of the POD coefficients; while the standard deviations are the same the resulting fields will be different since the noise does not act on the same quantities (POD coefficients versus displacement values).

Another uncertainty in the identification process is due to uncertainty in the other input parameters of the plate model such as the thickness. Other sources of uncertainty, such as misalignment of the center of the hole or misalignment of the loading direction can also be present. These could also be accounted for in the Bayesian identification by a more complex parameterization of the numerical finite element model. We directly parameterized uncertainty in the thickness of the plate h, which was assumed to be distributed normally with a mean value of 0.78 mm (the prescribed specimen thickness) and a standard deviation of 0.005 mm (the typical accuracy of a microcaliper). Alignment uncertainty as well as other sources of modeling uncertainty were considered indirectly, with somewhat decreased fidelity through a generic uncertainty term on the POD coefficients that had zero mean and a standard deviation of 0.4% of the mean value of the POD coefficients. For more details on the uncertainty modeling refer to [15].

5.2 Numerical procedure

The expensive part in the Bayesian identification approach used is the calculation of the likelihood function, since Monte Carlo simulations are used. The POD method and response surface methodology served for reducing the cost associated with the construction of the likelihood function. A flowchart overview of the utilized procedures is presented in Figure 8.
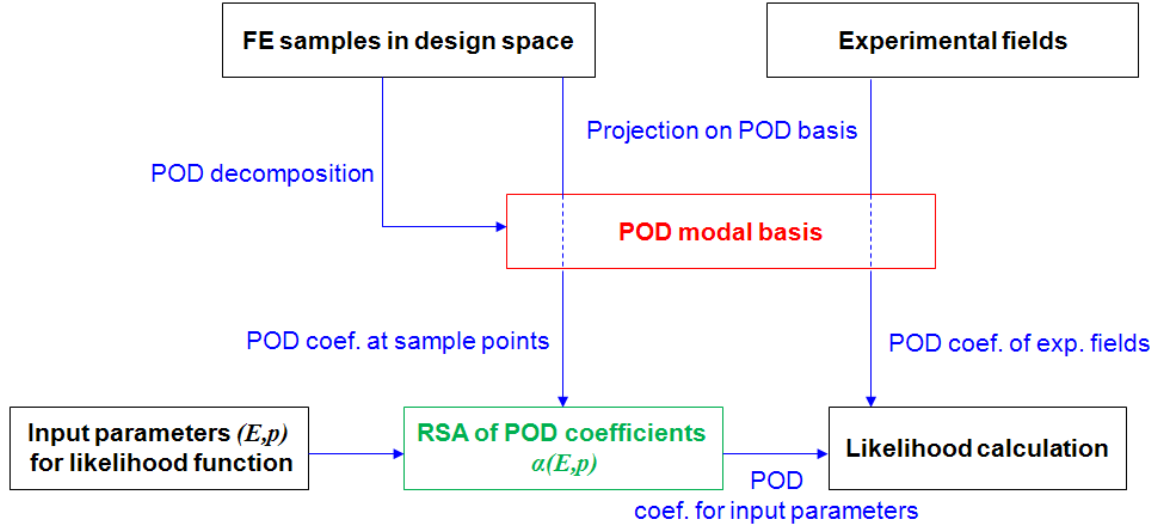
Figure 8. Flow chart of the procedure used to calculate the likelihood function. Cost reduction is shown in green and dimensionality reduction in red.

The likelihood function is computed point by point within the prior distribution's support (truncation bounds) at a grid in the four-dimensional space of the material properties $E = \{ E_1, E_2, v_{12}, G_{12} \}$. We chose a 17^4 grid, which is a compromise between convergence and computational cost considerations.

At each of the grid points, E is fixed and we need to evaluate the probability density function (PDF) of the POD coefficients, $f_{\alpha|E=E^{fixed}}(\alpha)$, at the point $\alpha = \alpha^{measure}$. The PDF of the POD coefficients is determined by propagating through Monte Carlo with 4000 simulations the uncertainties in the plate thickness and adding a sampled value of the normally distributed uncertainty in the POD coefficients resulting from measurement and modeling uncertainty, as described in the previous subsection.

Physical considerations showed that the resulting samples must be close to Gaussian so the samples were replaced by the normal distribution, having the sample mean and variance-covariance matrix. This Gaussian nature is due to the fact that the uncertainty resulting from the measurement noise is Gaussian and the uncertainty due to thickness is proportional to $1/h$, which can in this case be well approximated by a normal distribution. The distribution $f_{\alpha|E=E^{fixed}}(\alpha)$ was then evaluated at the point $\alpha = \alpha^{measure}$, leading to $f_{\alpha|E=E^{fixed}}(\alpha^{measure})$. In this way we obtain a discretized likelihood function, which multiplied by the prior distribution gives us the posterior distribution of the elastic constants that we seek to identify.

At this point we want to make the following note. We found that the overall uncertainty on the POD coefficients is close to normal, which means that the Bayesian identification could have been treated within a purely analytical framework, thus avoiding the need for expensive Monte Carlo simulations. The analytical treatment would however have no longer been possible if uncertainties on other input parameters would have been considered leading to a clearly non-Gaussian distribution on the POD coefficients. In such a case the Monte Carlo simulations based approach would still work and we kept it here for generality.

The Bayesian numerical procedure was first tested on a simulated experiment where good agreement between the true values and most likely identified values of the properties was found. For details on the identification on the simulated experiment the reader can refer to [15].

5.3 Identification results and discussion

The Bayesian framework does not identify a single value for each of the four ply-elastic constants but a probability distribution function characterizing the properties as well as the uncertainties with which these are obtained. Applying the Bayesian procedure to the experimental displacement fields described in Section 2 leads to the four-dimensional joint probability distribution characterized by the mean value, coefficient of variation and correlation given in Tables 9 and 10.

Table 9. Mean values and coefficient of variation of the identified posterior distribution based on the Moiré interferometry full fields from an open hole tensile test.

Parameter	E_1 (GPa)	E_2 (GPa)	ν_{12}	G_{12} (GPa)
Mean value	138	7.48	0.33	5.02
COV (%)	3.1	9.5	10.3	4.3

Table 10. Correlation matrix (symmetric) of the identified posterior distribution based on the Moiré interferometry full fields from an open hole tensile test.

	E_1	E_2	ν_{12}	G_{12}
E_1	1	0.020	-0.045	0.52
E_2	-	1	-0.005	-0.17
ν_{12}	-	-	1	0.24
G_{12}	-	-	-	1

We note first that the coefficients of variation with which the properties are identified vary greatly from one property to another. While the longitudinal Young's modulus E_1 of the ply is identified most accurately, the Poisson's ratio ν_{12} of the ply is identified with the highest uncertainty. This trend has been often noted in the composites community, since repeated tests on a same specimen typically lead to much higher dispersion in some properties than in others (Poisson's ratio and shear modulus are typically known more poorly. E_2 is identified here with a higher uncertainty than G_{12}. This is due to the stacking sequence $[45,-45,0]_s$, which does not have a 90° ply, thus making it more difficult to identify E_2 from the traction test in the 1-direction.

We also note that some of the correlation coefficients are significant. This is an important result and we could not find any previous study giving the correlation matrix of the orthotropic constants identified. Ignoring the correlation would lead to significantly overestimating the uncertainty in the identified properties. The results of Tables 9 and 10 can thus provide a more realistic model of experimental uncertainty compared the uncorrelated models that are often used in probabilistic studies.

Finally, looking at the mean values of the identified distribution we note a good agreement with the manufacturer's specifications, except for E_1. This might seem surprising, however Noh [18] found a similar value on the exact same prepreg roll that we used (cf. Table 1). The mean values of E_2, ν_{12} and G_{12} are close to the specification values. G_{12} is far however from Noh's values but it should be noted that the four point bending test is relatively poor for identifying G_{12}.

Thus, while it might seem surprising that the property that is identified with the lowest uncertainty (E_1) is also the one which is the furthest away from the manufacturer's specifications, it is important to recall that the identification does not account for inter-specimen variability or inter-prepreg batch variability of the material properties. Thus if the specimen deviates somewhat from the manufacturer's specification, it is not contradictory that, while identifying a property far away from the specifications, this can still be the property identified with the lowest uncertainty. The other variabilities, not identified by the Bayesian method, would then have to be estimated by repeating tests on multiple specimens coming from different prepreg rolls.

On a final note, probabilistic studies in structural design often use variability models in order to estimate the probability of failure. The variability can be estimated or propagated through the physics of the problem. In all the cases an important part of the total uncertainty stems from the measurements. Uncorrelated uncertainty models are often used for the experimental uncertainty due to lack of better estimates and this can lead to errors in the probability of failure. The Bayesian identification approach offers the possibility to improve the models of experimental uncertainty by providing correlation data. Initial studies on the impact of the correlation models on experimental uncertainty are presented in [19].

6 Conclusions

We considered in the present article the problem of orthotropic elastic constants identification based on full field displacement measurements on a plate with a hole. Moiré interferometry was carried out during the open hole tensile test and provided the experimental data for the identification. Bayesian identification was used in order to identify a probability distribution for the ply-elastic constants, thus characterizing the uncertainty with which the properties can be found from the given open hole tensile on the given specimen.

In order to make the Bayesian approach computationally feasible for the considered problem we had to solve two issues: the high dimensionality of the measurement data and the computational cost of the numerical model. These issues were addressed by using proper orthogonal decomposition to drastically reduce the dimensionality of the fields and by using response surface methodology to replace the expensive finite element simulations.

The identified probability distribution showed that the four orthotropic elastic constants are not identified with the same confidence. While the longitudinal Young's modulus was identified with the lowest standard deviation, the Poisson's ratio was identified with the highest uncertainty. Furthermore the properties were identified with non-negligible correlation. The Bayesian approach allowed to quantify these various items (mean values, standard deviations, correlations).

The longitudinal Young's modulus was also found to be far away from the manufacturer's specifications. This was consistent however with previous test results on the same prepreg roll using traditional four point bending tests.

Finally, it is important to note that the distribution determined by Bayesian identification is only part of the total uncertainty present in design problems and additional variability need to be determined by repeating tests multiple times.

Acknowledgements

References

1. Avril, S., Bonnet, M., Bretelle, A.S., Grédiac, M., Hild, F., Ienny, P., Latourte, F., Lemosse, D., Pagano, S., and Pagnacco, E., *Exp. Mech.,* **48**, 4 (2008).
2. Kaipio, J.P., and Somersalo, E. *Statistical and computational inverse problems.* (Springer, New York, 2005).
3. Gogu, C., Haftka, R.T., Le Riche, R., Molimard, J., Vautrin, A., *An Introduction to the Bayesian Approach Applied to Elastic Constants Identification*, *AIAA Journal*, In Press, (2009)
4. Isenberg, J., *Proc. of ASME Design Engineering Technical Conferences*, (1979)
5. Sol, H., *Identification of anisotropic plate rigidities*, PhD dissertation (Vrije Universiteit Brussel, 1986)

6. Lai, T.C. and Ip, K.H., *Composite Structures*, **34**, (1996)
7. Gogu, C., Haftka, R. T., Le Riche, R., Molimard, J., Vautrin, A., Sankar, B. V., *Proc. 11ᵗʰ AIAA Non-Deterministic Approaches Conference*, Palm Springs, CA, (2009)
8. Lecompte, D., Sol, H., Vantomme, J., and Habraken, A. M., *Proc. SEM Annual Conf. and Exposition on Experimental and Applied Mechanics*, (2005).
9. Silva, G., Le Riche, R., Molimard, J., Vautrin, A., and Galerne, C., *Adv. Exp. Mech.*, **7-8**, (2007).
10. Post, D., Han, B., and Ifju, P., *High sensitivity moiré: experimental analysis for mechanics and materials.* (Springer, New York, 1997).
11. Walker, C.A., *Experimental Mechanics,* **34**, 4, (1994).
12. Yin, W., *Automated strain analysis system: development and applications*. Ph.D. Dissertation Proposal, University of Florida, (2008).
13. Jolliffe I.T., *Principal component analysis*, 2ⁿᵈ edition, (Springer, New York, 2002).
14. Gogu C., Haftka, R.T., Le Riche, R., Molimard, J., Vautrin, A., *Proc. 17ᵗʰ International Conference on Composite Materials (ICCM17)*, Edinburgh, UK, (2009).
15. Gogu C., *Facilitating Bayesian Identification of Elastic Constants through Dimensionality Reduction and Response Surface Methodology,* PhD dissertation, University of Florida and Ecole des Mines de Saint Etienne, (2009).
16. Myers, R.H., and Montgomery, D.C., *Response Surface Methodology: Process and Product in Optimization Using Designed Experiments.* (John Wiley & Sons, New York, 2002).
17. Allen, D. M., *Technometrics,* **13**, (1971).
18. Noh, W.J., *Mixed Mode Interfacial Fracture Toughness of Sandwich Composites at Cryogenic Temperatures*, Master's Thesis, University of Florida, (2004).
19. Smarslok, B.P., Haftka, R.T., and Ifju, P., *Proc. 23ʳᵈ Annual Technical Conference of the American Society for Composites*, Memphis, TN, (2008).